18th Brazilian Congress of Thermal Sciences and Engineering
November 16-20, 2020 (Online)

ENCIT2020-0143
THE VENTILATION DUCT SHAPE INFLUENCE ON THE PARTICLE DEPOSITION IN A 90° BEND

Marcos Batistella Lopes
Diego Barreto Pedroso Simões
Viviana Cocco Mariani
Pontifical Catholic University of Paraná, PPGEM, R. Imaculada Conceição, 1155, Curitiba, 80215-901, Brazil
marcos.batistella@pucpr.edu.br
diegosimoes1@hotmail.com
viviana.mariani@pucpr.br

Abstract. *This study performs numerical modelling using the Eulerian-Lagrangian method to study the influence of the duct cross-section on deposition rates for the monodisperse and dilute air-particle flow in a 90° duct bend. First, the airflow with a Reynolds number of 40,000 through a square 90° duct bend with the hydraulic diameter of 0.08m and the curvature ratio of 4 was validated against the literature applying the SST k-ω eddy-viscosity model. Then, the square duct bend airflow field was compared in terms of the mean velocity and the turbulent kinetic energy with a circular duct operating with the same flow conditions. Finally, the particle deposition rates on the circular and square duct bend for the particle size between 0.1μm and 100μm comparing with the correlations from literature. The deposition rates were higher on the circular duct bend than the square duct bend for the Stokes number ranging from 0.4 to 3.0.*

Keywords: *airflow, duct bend, particle deposition, Eulerian-Lagrangian approach*

1. INTRODUCTION

People spend most of their time in indoor environments and are exposed to a range of air contaminants (Liu et al., 2018). The aerosols size in ventilation ducts is up to 100μm and particles less than 2.5μm can get deep into the lungs causing serious health problems (ASHRAE, 2017). In mechanically ventilated and conditioned buildings, the particle concentration within the building environment can be affected by the duct system. The particle deposition is lower on straight ducts than on fittings such as the ventilation elbows (Jeong et al., 2009). Normally, numerical modeling of gas-solid flows is carried out with Eulerian-Eulerian or Eulerian-Lagrangian methods (Crowe et al., 2017). Since the aerosol concentration in ventilated rooms must be small (the particle volume fraction is lower than 10^{-6}), we have diluted flow and the Eulerian-Lagrangian approach can be chosen to perform this study.

Handling with the Eulerian-Lagrangian approach implies the carrier phase (the air) must be properly modeled. The airflow in curved pipes is more complex than in straight pipes because secondary flows occur as well as the flow separation in the inner bend wall (Spedding et al., 2004). The turbulence modeling of the airflow in curved pipes requires special attention due to the presence of curved streamlines. The literature shows the Large Eddy Simulation (LES) models are accurate to predict this complex flow such as shown by Tanaka et al. (2009). However, most of the literature was carried out with the Reynolds Averaged Navier-Stokes (RANS) closure models due to the computation resources available such as the Re-Normalization Group k-ε model (Kim et al., 2014) and the Reynolds Stress Models (Bluestein et al., 2019).

Particle deposition rates on curved pipes have been numerically studied usually with one-way coupling (Elghobashi, 1994) and a Lagrangian particle tracking model for the disperse phase (the aerosol) integrating an eddy lifetime model to consider the velocity fluctuations of the carrier phase into the forces acting on the particles (Mofakham and Ahmadi, 2020). To avoid modelling all the complexities of the particle-wall interactions (Almohammed and Breuer, 2016) the stick condition is largely applied, i.e., the particles are deposited once in contact with the pipe walls (Breuer et al., 2006; Berrouk and Laurence, 2008; Zhang et al., 2012; Gao and Li, 2012; Guo et al., 2020).

The present study seeks to assess the influence of the duct shape (square and circular ducts) on the particle deposition in 90° bends. First, the turbulent airflow through a square-sectioned 90° bend with a hydraulic diameter (D_h) of 0.08m, a curvature ratio (δ) of 4, and a Reynolds number (Re) of 4×10^4 was validated against the work of Sudo et al. (2001). Then, a monodisperse cloud of particles was injected and tracked into the previous airflow solution and the deposition rates were compared with a circular duct with the same flow conditions (i.e., the same D_h, δ, and Re) and validated with the correlations proposed by Pui et al. (1987) and McFarland et al. (1997).

2. MODEL

The physical model is a 90° bend that connects a horizontal to horizontal straight ducts as illustrated in Fig. 1. In this figure: D_h is the hydraulic diameter (D_h = 0.08m), R_b is the bend radius (R_b = 0.16m, consequently the curvature ratio, δ, is $\delta = 2R_b/D_h = 4$), α_b is the bend angle, g_z is the gravity direction (g_z = 9.81ms^{-2}), L_1 and L_2 are, respectively, the length of the straight ducts upstream and downstream the bend ($L_1 = L_2$ = 4m).

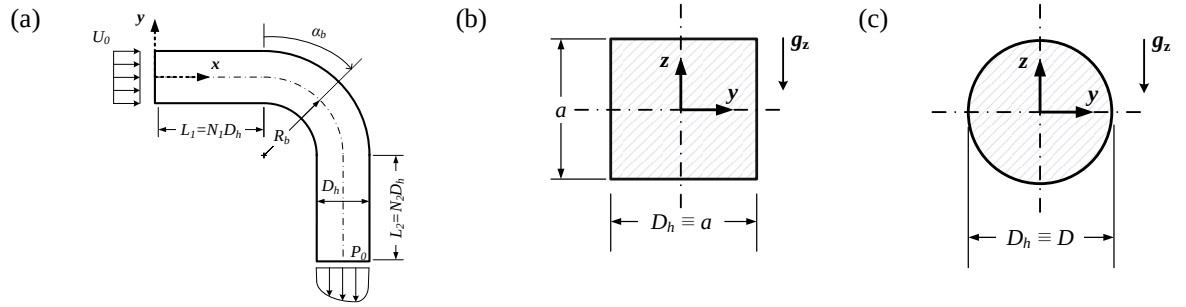

Figure 1. Geometry and boundary conditions for the duct bend: (a) top view, (b) square duct, and (c) circular duct.

The turbulence variables and the velocity profiles were assumed constant at the inlet of the domain (U_0 = 7.4ms^{-1} and 5% of turbulence intensity) leading to the Reynolds number of 4×10^4. The pressure at the outlet of the domain is constant (P_0 = 1atm). The wall was considered with a non-slip boundary condition. The zero gradient boundary condition was set to the pressure at the domain inlet and the walls as well as the velocity and the turbulence variables at the domain outlet. One cloud with 10^5 monodispersed particles of 2.5×10^3kgm^{-3} density was injected at once with the same local air velocity in the upstream duct near the bend inlet (x/D_h = 40), for a particle size ranging from 0.1μm to 100μm, and the particles were tracked until all particles cross the bend outlet with the time step of 10^{-6}s.

2.1 Carrier phase

The RANS equations are obtained by averaging the transport equations. If the airflow is statistically steady and incompressible, the mass conservation and momentum transport equations can be expressed by Eqs. (1) and (2) (Ferziger et al., 2020):

$$\nabla \cdot \vec{u} = 0 \tag{1}$$

$$\frac{\partial \overline{u}_i}{\partial t} + \nabla \cdot \left(\overline{u}_i \vec{u} \right) = -\frac{1}{\rho} \nabla \cdot \left(\overline{p} \vec{i}_i \right) + \nabla \cdot \left(\nu \nabla \overline{u}_i - \overline{u_i' u_j'} \right) \tag{2}$$

where $\vec{u}$ is the mean fluid velocity (ms^{-1}), t is the time (s), ρ is the fluid density (kgm^{-3}), $\overline{p}$ is the mean pressure (Pa), ν is the kinematic fluid viscosity (m^{2}s^{-1}), $\vec{i}_i$ is the Cartesian unit vector at the direction i, and $\overline{u_i' u_j'}$ is the Reynolds stress tensor (m^{2}s^{-2}).

The eddy-viscosity models assume that the Reynolds stress tensor is proportional to the strain tensor as proposed by Kolmogorov:

$$-\overline{u_i' u_j'} = 2\nu_t \overline{S}_{ij} - \frac{2}{3} k \delta_{ij} \tag{3}$$

where ν_t is the turbulent kinematic viscosity, S_{ij} is the mean strain rate tensor given by:

$$\overline{S}_{ij} = \frac{1}{2} \left(\frac{\partial \overline{u}_i}{\partial x_j} + \frac{\partial \overline{u}_j}{\partial x_i} \right) \tag{4}$$

k is the turbulent kinetic energy defined as:

$$k = \frac{1}{2}\overline{u_i' u_i'} \tag{5}$$

and δ_{ij} is the Kronecker delta.

The eddy-viscosity model applied in this study is the Shear Stress Transport (SST) k-ω model developed by Menter et al. (2006) because this model has good behavior in adverse pressure gradient and separating flow, and has been performed well to predict the turbulent airflow in duct bends as shown by the authors in previous studies (Lopes and Mariani, 2017; Lopes et al., 2018; Lopes et al., 2020). For the sake of brevity, the additional transport equations for the turbulent kinetic energy (k) and the turbulence frequency (ω), and the kinematic eddy viscosity (ν_t), of the SST k-ω turbulence model will not be presented here and you can find them in Versteeg and Malalasekera (2007).

2.2 Disperse phase

The equations of the particle motion in the turbulent flow for the Lagrangian method with one-way coupling can be expressed as (Crowe et al., 2017):

$$\frac{d\vec{x}_p}{dt} = \vec{u}_p \tag{6}$$

$$m_p \frac{d\vec{u}_p}{dt} = \sum_i \vec{F}_i \tag{7}$$

where $\vec{x}_p$ is the particle position (m), $\vec{u}_p$ is the particle instantaneous velocity (ms^{-1}), m_p is the particle mass (kg), and $\vec{F}$ are forces acting on particles (N).

Since the ratio between the fluid and the particle density is small in this study, the Basset, the virtual mass, and the pressure-gradient forces were neglected. Consequently, the main forces acting on the particles are gravity and drag forces. The shear-lift force is also considered as well as the Brownian diffusion for the submicron particles.

The gravity force ($\vec{F}_g$) is calculated as:

$$\vec{F}_g = m_p \left(1 - \frac{\rho}{\rho_p}\right)\vec{g} \tag{8}$$

where $\vec{g}$ is the gravity acceleration at z-direction, ρ is the fluid density, and ρ_p is the particle density.

The drag force ($\vec{F}_d$) is the resistance of the fluid to the particle motion defined as:

$$\vec{F}_d = -C_d \frac{1}{8}\rho\pi {d_p}^2 \left|\vec{u}_p - \vec{u}\right|\left(\vec{u}_p - \vec{u}\right) \tag{9}$$

where d_p is the particle diameter, $\vec{u}$ is the instantaneous fluid velocity at particle location, and C_d is the drag coefficient determined as (Putnam, 1961):

$$C_d = \begin{cases} \dfrac{24}{\mathrm{Re}_p}\left(1 + \dfrac{\mathrm{Re}_p^{2/3}}{6}\right) & , \quad if \quad \mathrm{Re}_p \le 10^3 \\ 0.424 & , \quad if \quad \mathrm{Re}_p > 10^3 \end{cases} \tag{10}$$

where Re_p is the particle Reynolds number ($\mathrm{Re}_p = \left|\vec{u}_p - \vec{u}\right| d_p / \nu$).

The shear-lift force ($\vec{F}_l$) is the component of the force acting on the particle perpendicular to the main flow direction due to the inertial effects in the viscous flow around the particle surface. An expression for the shear-lift force was proposed by Saffman (1965; 1968):

$$\vec{F}_{l(Saff)} = 1.615\rho\sqrt{\nu}d_p^{\,2}\left|\vec{u}_p - \vec{u}\right|\left(\left|\frac{\partial u}{\partial n}\right|\right)^{1/2}\operatorname{sgn}\left(\frac{\partial u}{\partial n}\right) \tag{11}$$

where n is the normal coordinate to the main flow direction.

The Saffman's shear-lift force ($\vec{F}_{l(Saff)}$) is valid only for low particle Reynolds number ($\mathrm{Re}_p << 1$). Therefore, a more general correlation was applied in this study, the shear-lift force proposed by Mei (1992):

$$\vec{F}_l = 1.615\rho\sqrt{\nu}d_p^{\,2}\left[\left(\vec{u} - \vec{u}_p\right)\times\vec{\omega}\right]\left(\frac{1}{|\vec{\omega}|}\right)^{1/2} C_l \tag{12}$$

where $\vec{\omega}$ is the local vorticity of the fluid ($\vec{\omega} = \nabla\times\vec{u}$) and C_l is the coefficient given by:

$$C_l = \begin{cases} \left(1 - 0.3314\sqrt{\alpha}\right)\exp\left(-\mathrm{Re}_p/10\right) + 0.3314\sqrt{\alpha} & , \quad if \quad \mathrm{Re}_p \le 40 \\ 0.0524\sqrt{\alpha\,\mathrm{Re}_p} & , \quad if \quad \mathrm{Re}_p > 40 \end{cases} \tag{13}$$

where α is the dimensionless shear rate ($\alpha = \left(d_p/2\right)|\vec{\omega}|/|\vec{u} - \vec{u}_p|$).

Submicron particles (d_p < 1μm) are affected by the influence of the Brownian motion, i.e., since submicron particle size is of the order of the air mean free path (~70nm), the air molecules moving randomly change the trajectories of the submicron particles. Therefore, the Brownian diffusion can be represented by a source term in the Eq. (7). The Brownian force (F_B) can be expressed according to Li and Ahmadi (1992):

$$F_B = \rho_p\frac{\pi}{6}d_p^{\,3}\zeta\left(\frac{\pi S_0}{\Delta t}\right)^{1/2} \tag{14}$$

where ζ is a zero-mean, unit-variance-independent Gaussian random number, Δt is the time step size in which the amplitude of Brownian forces component is evaluated, and S_0 is the spectral density of a Gaussian white noise random process given as:

$$S_0 = \frac{216\nu k_B T}{\pi^2\rho d_p^{\,5}\left(\rho_p/\rho\right)^2 C_C} \tag{15}$$

where k_B is the Boltzmann constant ($k_B = 1.38\times10^{-23}\,J/K$), T is the temperature, and C_C is the Stokes-Cunningham slip correction factor defined as:

$$C_C = 1 + \left(\frac{2\lambda}{d_p}\right)\left[1.257 + 0.4\exp\left(-\frac{0.55d_p}{\lambda}\right)\right] \tag{16}$$

where λ is the air mean free path.

To calculate the forces acting on particles, the instantaneous fluid velocity seen by the particle is needed. Since the RANS models calculated only the time-averaged fluid velocity, a stochastic model must be applied to calculate the instantaneous fluid velocity at particle location. The stochastic model of Gosman and Ionnides (1983) was used in this study in which the velocity fluctuation of the fluid-phase ($\vec{u}'$) when the particle crosses a turbulent eddy is defined as:

$$\vec{u}' = \zeta\left(\frac{2}{3}k\right)^{1/2}\vec{dir} \tag{17}$$

where $\vec{dir}$ is a random vector. The Eq. (7) is integrated until the particle does not interact anymore with the same eddy. The interaction duration of the particle with the eddy (τ_i) is calculated between the eddy lifetime (τ_e) and the time for the particle pass through the eddy (τ_r):

$$\tau_i = \min\left[\tau_e , \tau_r\right] \tag{18}$$

where τ_e is given by:

$$\tau_e = \frac{k}{\varepsilon} \tag{19}$$

where ε is the dissipation rate of the turbulent kinetic energy, and τ_r is the residence time of the particle in the eddy defined as:

$$\tau_r = \frac{C_r \dfrac{k^{3/2}}{\varepsilon}}{\left|\vec{u} - \vec{u}_p\right|} \tag{20}$$

where C_r is a constant.

2.3 Numerical procedure

The numerical solution of the governing equations for the fluid flow (Eqs. (1) and (2)) and the particle motion (Eqs. (6) and (7)) was solved with the toolbox OpenFOAM® (Greenshields, 2018). In OpenFOAM®, the Navier-Stokes equations are solved with the Finite Volume Method (FVM) using the cell-centered collocated variable arrangement. The PISO (Pressure Implicit with Splitting of Operators) algorithm (Issa, 1986) was used for the pressure-velocity coupling of the incompressible fluid flow until the steady solution was obtained. The convective terms were discretized with a second-order accurate numerical scheme, a fully orthogonal scheme was used for the diffusive terms, and the gradients terms were computed with the Gauss method. Once the flow was converged, particles were injected and tracked by analytical integration using the Lagrangian method and one-way coupling (i.e., only the fluid flow affects the particle trajectories while the particles do not affect the fluid flow).

The mesh was generated with the *blockMesh* tool. The grid convergence study was performed with three meshes for both square and circular ducts as listed in Tab. 1. Figure 2 presents the non-uniform structure mesh for both cases (*Grid 2*). The refinement expansion ratio regarding the number of nodes (N) from *Grid 1* to *Grid 2* and from *Grid 2* to *Grid 3* is near 1.2 following the Grid Convergence Index (GCI) method proposed by Roache (1994). The dimensionless distance normal to the wall was also observed and the maximum y^+ was lower than 1 for all grids (with at least 5 nodes in the viscous sublayer).

The average pressure drop (Δp) and the Darcy-Weisbach friction factor (f) were calculated for all meshes (Tab. 1). The pressure drop of the duct bend model (Fig. 1) is near 82Pa and the Darcy-Weisbach friction factor is near 0.0220. The relative error (E_r) is lower towards the finest grid in both ducts showing the convergence regarding these variables. Moreover, no significant variation of these flow properties was observed in both cases.

Table 1. Grid convergence study.

Cross-section		N	Δp [Pa] (E_r)	f (E_r)
Square	*Grid 1*	0.43×10^6	66.30 (-19%)	0.0125 (-43%)
	Grid 2	0.75×10^6	68.92 (-16%)	0.0131 (-40%)
	Grid 3	1.34×10^6	71.52 (-13%)	0.0136 (-38%)
Circular	*Grid 1*	0.48×10^6	66.86 (-19%)	0.0129 (-41%)
	Grid 2	0.88×10^6	70.10 (-15%)	0.0135 (-39%)
	Grid 3	1.61×10^6	70.77 (-14%)	0.0137 (-38%)

Figure 3 shows the air mean streamwise velocity at the bend outlet normalized with the bulk velocity. The dimensionless radius (r^*) ranges from the inner bend wall ($r^* = 0$) to the outer bend wall ($r^* = 1$). Almost no difference between the meshes was observed towards the outer bend wall region ($r^* > 0.5$). Near the inner bend wall region ($r^* < 0.3$), there was a convergence from the coarse grid to the fine grid. Therefore, the *Grid 3* was selected for further analysis.

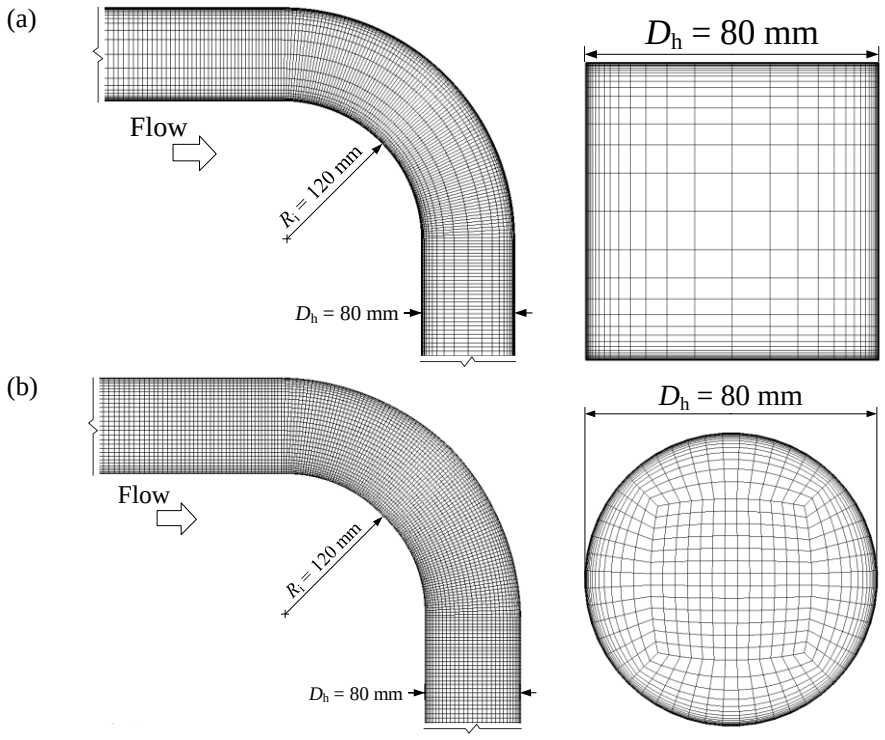

Figure 2. *Gird 2*: (a) the square and (b) the circular duct bend.

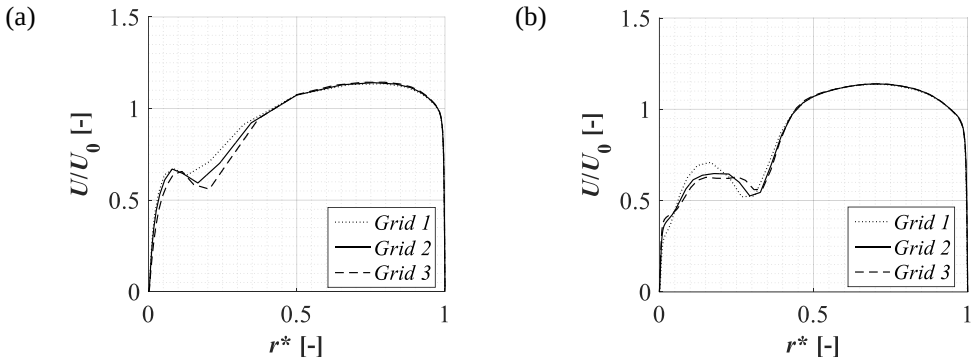

Figure 3. Grid convergence study: the streamwise mean air velocity at the bend outlet (α_b = 90°) for the (a) square and (b) circular duct.

3. RESULTS AND DISCUSSION

3.1 Fluid-phase

Figure 4 presents the validation of the fluid-phase regarding the mean streamwise velocity profiles. Only the square-sectioned duct is presented because the benchmark for validation was the work of Sudo et al. (2001). Figure 4a indicates the fully developed turbulent flow profile was close to the data from Klebanoff (1954) in which the mean streamwise velocity is normalized with the wall-friction velocity ($u_\tau = \sqrt{\tau_w/\rho}$), i.e., $u^+ = \bar{u}/u_\tau$, and the dimensionless distance normal to the wall is given by: $y^+ = yu_\tau/\nu$, where y is the normal distance to the wall. The velocity profile at the bend outlet is shown in Fig. 4b in which the dimensionless radius (r^*) can be defined as:

$$r^* = \frac{r - R_i}{R_o - R_i} \tag{21}$$

where r is the distance from the bend center to a position between the inner (R_i) and outer (R_o) bend radius.

The SST k-ω eddy-viscosity model was accurate enough to predict the velocity profile (Fig. 4b) corresponding to the Root Mean Square Error (RMSE) of only 8%.

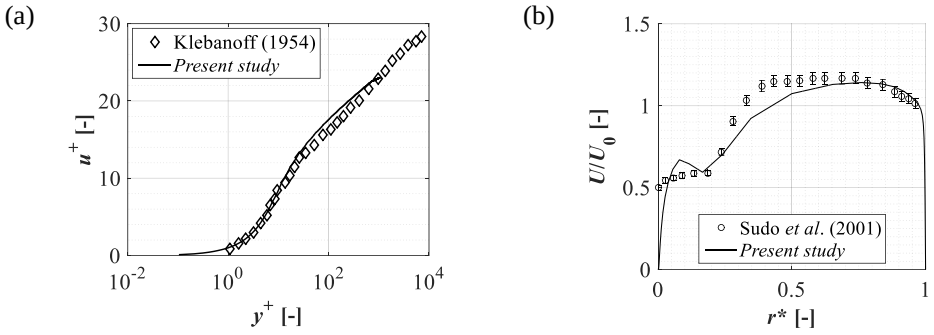

Figure 4. Square duct: (a) fully turbulent developed profile at the upstream straight duct close to the bend inlet (x/D_h = 45) and (b) mean streamwise velocity at the bend outlet (α_b = 90°).

Figure 5 proposes the comparison of the flow field between the square (Fig. 5a) and the circular (Fig. 5b) duct bend for the middle plane (z = 0) and some cross-section planes along the duct. For both square and circular ducts, the mean velocity profile was fully developed in the upstream duct near the bend inlet region (α_b = 0°). In addition, the mean velocity profile was disturbed in the duct bend and the downstream duct near the bend outlet region (α_b = 90°) offsetting the maximum velocity towards the outer bend wall. The flow separation region in the inner bend wall close to the bend outlet was larger in the circular duct (Fig. 5b) than in the square duct (Fig. 5a). As presumed, a stagnation region appears at the corners of the square duct, and due to the round geometry of the circular duct, no stagnation region was observed in this duct. The turbulent kinetic energy is higher at the middle plane in the downstream duct for the circular duct (Fig. 5b) than for the square duct (Fig. 5a). On the other hand, a region with higher turbulent kinetic energy was observed in the duct top wall at the bend outlet for the square duct.

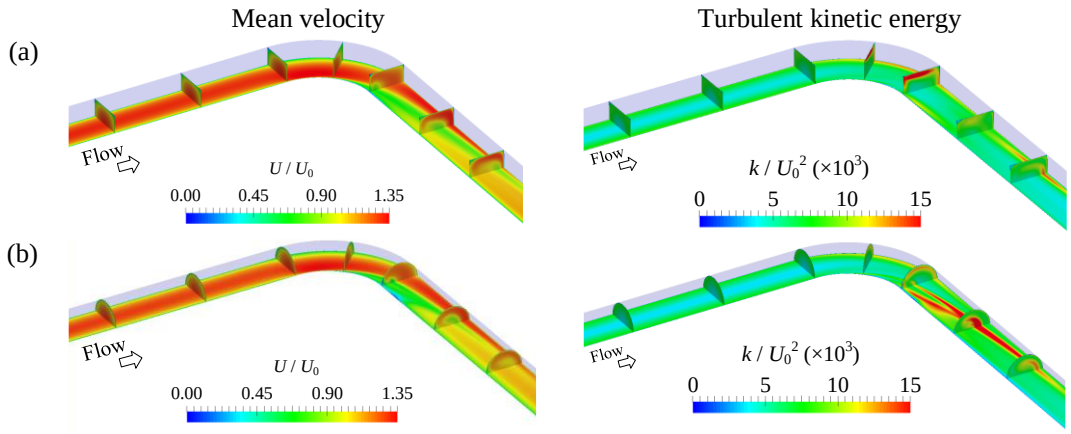

Figure 5. Comparison of the mean velocity and the turbulent kinetic energy contours for (a) square and (b) circular duct.

3.2 Particle-phase

Air-particle flows with important deposition rates as in this study can be analyzed using the collection efficiency (η) defined as:

$$\eta = 1 - \frac{C_o}{C_i} \tag{22}$$

where C_o and C_i are the particle concentration at the bend outlet and bend inlet, respectively. Once the air-particle flow is monodispersed, the concentration is represented by the number of particles, i.e., in this study C_i is the number of particles that enter the bend and C_o is the number of particles that exit the bend (the non-deposited particles).

Figure 6 presents the particle deposition collection efficiency validated against the experimental correlations from the circular ducts bend carried out by Pui et al. (1987) and McFarland et al. (1997). For particle size ranging from 0.1μm to 100μm, the corresponding Stokes number is 2×10^{-3} to 14, respectively. The Stokes number (St) is the ratio between the characteristic time scales defined as: $St = \tau_p / \tau_F$, where τ_F is the flow time scale ($\tau_F = (D_h/2)/U_0$) and τ_p is the particle response time given by:

$$\tau_p = \frac{C_C \rho_p d_p^{\,2}}{18\mu} \tag{23}$$

where μ is the dynamic viscosity of the air.

For both square and circular ducts of this study, Fig. 6 shows the lighter particles ($St \leq 0.1$) were almost all transported by the turbulent airflow through the duct bend, therefore the collection efficiency is close to 0% (without particle deposition on the duct bend walls). On the other hand, almost all heavier particles ($St \geq 2$) were deposited on the duct bend walls leading to the collection efficiency near 100% (all particles are deposited on the duct bend walls). These behaviors of the curves agreed with the experimental data from the literature. The collection efficiency of the circular duct bend of this study was higher for the circular duct bend than the square duct bend when the Stokes number ranges from 0.4 to 3.0.

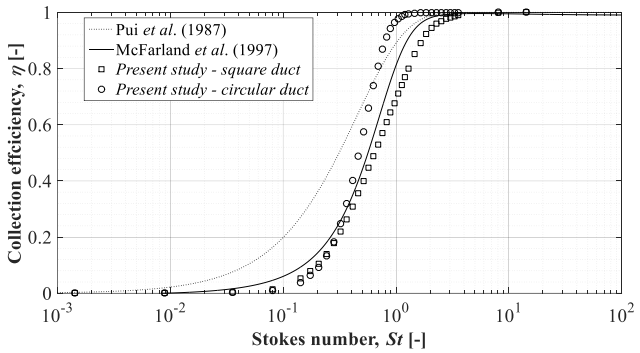

Figure 6. Particle deposition efficiency in the duct bend.

The particle deposition velocity (other property of the deposition rate) can be estimated as (Gao and Li, 2012):

$$V_d = -\frac{U_0}{3\pi} \ln\left(\frac{C_o}{C_i}\right) \tag{24}$$

The particle deposition velocity is normalized with the wall-friction velocity ($V_d^{+} = V_d / u_\tau$) and the particle relaxation time is normalized with the eddy lifetime ($\tau_p^{+} = \tau_p / \tau_e$). Figure 7 presents the dimensionless deposition velocity of this study compared with Wood's correlation (Wood, 1981) valid for $\tau_p^{+} < 10$. The behavior of this curve agreed with the literature and the three characteristics regimes were observed: the turbulent diffusion regime ($\tau_p^{+} < 2$), the eddy-diffusion impaction regime ($2 \leq \tau_p^{+} \leq 50$), and the particle inertia moderate regime ($\tau_p^{+} > 50$).

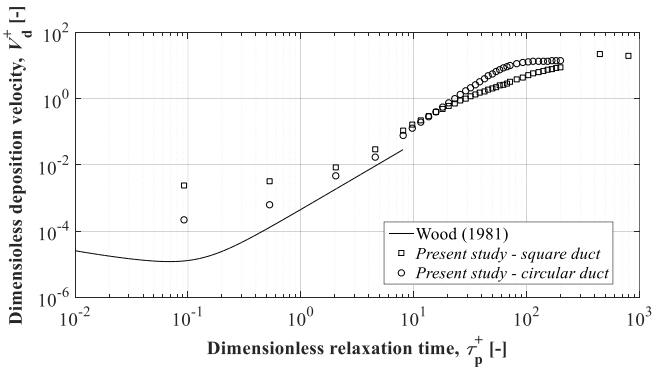

Figure 7. Particle deposition velocity in the duct bend.

4. CONCLUSIONS

This study carried out a numerical analysis with the Eulerian-Lagrangian approach using the code OpenFOAM® to solve the governing equations of the incompressible fluid flow and the particle transport for a 90° duct bend air-particle diluted flow within a circular and a square ducts. First, the turbulent airflow was solved with the SST k-ω eddy-viscosity model validating against the available literature and comparing the airflow field of the circular and square ducts. Then, a Lagrangian model with one-way coupling was incorporated in the previous airflow solutions to determine the deposition rates for the particle size ranging from 0.1μm to 100μm. Overall, the flow separation region was larger in the circular duct than the square duct and the deposition rates were higher on the circular duct than the square duct for the Stokes number between 0.4 and 3.0. Future research can include a more realistic particle-wall interaction model and apply other turbulence models.

5. ACKNOWLEDGEMENTS

The authors would like to thank the National Council of Scientific and Technologic Development of Brazil - CNPq (Grants: 307966/2019-4-PQ, 405101/2016-3-Univ) and Fundação Araucária (PRONEX-FA/CNPq 042/2018) for its financial support of this work.

6. REFERENCES

Almohammed, N. and Breuer, M., 2016. “Modeling and simulation of particle-wall adhesion of aerosol particles in particle-laden turbulent flows”. *International Journal of Multiphase Flow*, Vol. 85, pp. 142–156.

ASHRAE, 2017. *ASHRAE Handbook: Fundamentals*. American Society of Heating, Refrigeration and Air-Conditioning Engineers, USA, SI edition.

Berrouk, A.S. and Laurence, D., 2008. “Stochastic modelling of aerosol deposition for LES of 90° bend turbulent flow”. *International Journal of Heat and Fluid Flow*, Vol. 29, No. 4, pp. 1010–1028.

Bluestein, A.M., Venters, R., Bohl, D., Halenbrook, B.T. and Ahmadi, G., 2019. “Turbulent flow through a ducted elbow and plugged tee geometry: an experimental and numerical study”. *Journal of Fluids Engineering*, Vol. 141, No. 8, pp. 1-14.

Breuer, M., Baytekin, H.T. and Matida, E.A, 2006. “Prediction of aerosol deposition in bends using LES and an efficient Lagrangian tracking method”. *Journal of Aerosol Science*, Vol. 37, No. 11, pp. 1407–1428.

Crowe , C.T., Michaelides, E. and Schwarzkopf, J.D., 2017. *Multiphase Flow Handbook*. Taylor & Francis Group, Boca Raton, 2nd edition.

Elghobashi, S., 1994. “On predicting particle-laden turbulent flows”. *Applied Scientific Research*, Vol. 52, No. 4, pp. 309–329.

Ferziger, J.H., Perić, M. and Street, R.L., 2020. *Computational Methods for Fluid Dynamics*. Springer International Publishing, Cham, 4th edition.

Gao, R. and Li, A., 2012. “Dust deposition in ventilation and air-conditioning duct bend flows”. *Energy Conversion and Management*, Vol. 55, pp. 49–59.

Gosman, A.D. and Ionnides, E., 1983. “Aspects of computer simulation of liquid-fueled combustors”. *Journal of Energy*, Vol. 7, No. 6, pp. 482–490.

Greenshields, C.J., 2018. *OpenFOAM User Guide version 6*. OpenFOAM Foundation Ltd..

Guo, J., Chen, Z., Shen, B., Wang, J. and Yang, L., 2020. “Numerical study on characteristics of particle deposition efficiency on different walls of 90° square bend”. *Powder Technology*, Vol. 364, pp. 572–583.

Issa, R., 1986. “Solution of the implicitly discretised fluid flow equations by operator-splitting”. *Journal of Computational Physics*, Vol. 62, No. 1, pp. 40–65.

Jeong, J.-W., Bem, J., Bahnfleth, W.P., Freihaut, J.D. and Thran, B., 2009. “Critical review of aerosol particle transport models for building HVAC ducts”. *Journal of Architectural Engineering*, Vol. 15, No. 3, pp. 74–83.

Kim, J., Yadav, M. and Kim, S., 2014. “Characteristics of secondary flow induced by 90-degree elbow in turbulent pipe flow”. *Engineering Applications of Computational Fluid Mechanics*, Vol. 8, No. 2, pp. 229–239.

Klebanoff, P.S., 1954. “Characteristics of turbulence in a boundary layer with zero pressure gradient”. In *Report NACA-TR-1247*.

Li, A. and Ahmadi, G., 1992. "Dispersion and deposition of spherical particles from point sources in a turbulent channel flow". *Aerosol Science and Technology*, Vol. 16, No. 4, pp. 209–226.

Liu, Z., Ma, S., Cao, G., Meng, C. and He, B.J., 2018. "Distribution characteristics, growth, reproduction and transmission modes and control strategies for microbial contamination in HVAC systems: A literature review". *Energy and Buildings*, Vol. 177, pp. 77-95.

Lopes, M.B., Mariani, V.C., Mendonça, K.C. and Béghein, C., 2018. "Evaluating RANS turbulence models to predict the airflow in a duct bend". In *Proceedings of the 17th Brazillian Congress of Thermal Sciences and Engineering – ENCIT 2018.* Águas de Lindóia, Brazil.

Lopes, M.B., Mariani, V.C., Mendonça, K.C. and Béghein, C., 2020. "On the use of particle-wall interaction models to predict particle-laden flow in 90-deg bends". *Building Simulation*, pp. 1–17.

Lopes, M.B. and Mariani, V.C., 2017. "Particle deposition in a ventilation duct bend". In *Proccedings of the 24th ABCM International Congress of Mechanical Engineering – COBEM 2017*. Curitiba, Brazil.

McFarland, A.R., Gong, H., Muyshondt, A., Wente, W.B. and Anand, N.K., 1997. "Aerosol deposition in bends with turbulent flow". *Environmental Science & Technology*, Vol. 31, No. 12, pp. 3371–3377.

Mei, R., 1992. "An approximate expression for the shear lift force on a spherical particle at finite reynolds number". *International Journal of Multiphase Flow*, Vol. 18, No. 1, pp. 145–147.

Menter, F.R., Langtry, R. and Völker, S., 2006. "Transition modelling for general purpose CFD codes". *Flow, Turbulence and Combustion*, Vol. 77, No. 1–4, pp. 277–303.

Mofakham, A.A. and Ahmadi, G., 2020. "On random walk models for simulation of particle-laden turbulent flows". *International Journal of Multiphase Flow*, Vol. 122, pp. 103157.

Pui, D.Y.H., Romay-Novas, F. and Liu, B.Y.H., 1987. "Experimental study of particle deposition in bends of circular cross section". *Aerosol Science and Technology*, Vol. 7, No. 3, pp. 301–315.

Putnam, A., 1961. "Integrable form of droplet drag coefficient". *American Rocket Society Jornal*, Vol. 31, pp. 1467–1468.

Roache, P.J., 1994. "Perspective: A method for uniform reporting of grid refinement studies". *Journal of Fluids Engineering*, Vol. 116, No. 3, pp. 405–413.

Saffman, P.G., 1965. "The lift on a small sphere in a slow shear flow". *Journal of Fluid Mechanics*, Vol. 22, No. 2, pp. 385–400.

Saffman, P.G., 1968. "Corrigendum to "The lift on a small sphere in a slow shear flow"". *Journal of Fluid Mechanics*, Vol. 31, pp. 624.

Spedding, P.L., Benard, E. and McNally, G.M. "Fluid flow through 90 degree bends". *Developments in Chemical Engineering and Mineral Processing*, Vol. 12, No. 1–2, pp. 107–128.

Sudo, K., Sumida, M. and Hibara, H., 2001. "Experimental investigation on turbulent flow in a square-sectioned 90-degree bend". *Experiments in Fluids*, Vol. 30, No. 3, pp. 246–252.

Tanaka, M., Ohshima, H. and Monji, H., 2009. "Numerical investigation of flow structure in pipe elbow with large eddy simulation approach". In *Proceddings of the ASME 2009 Pressure Vessels and Piping. Volume 3: Design and Analysis*. Prague, Czech Republic.

Versteeg, H.K. and Malalasekera, W., 2007. *An Introduction to Computational Fluid Dynamics: The Finite Volume Method*. Pearson Education Limited, London. 2nd edition

Wood, N.B., 1981. "A simple method for the calculation of turbulent deposition to smooth and rough surfaces". *Journal of Aerosol Science*, Vol. 12, No. 3, pp. 275–290.

Zhang, P., Roberts, R.M. and Bénard, A., 2012. "Computational guidelines and an empirical model for particle deposition in curved pipes using an Eulerian-Lagrangian approach". *Journal of Aerosol Science*, Vol. 53, pp. 1–20.

7. RESPONSIBILITY NOTICE

The authors are the only responsible for the printed material included in this paper.